Transport Properties of Thermal Oxide Films Grown on Polycrystalline Silicon—Modeling and Experiments

CHING-YUAN WU, MEMBER, IEEE, AND CHIOU-FENG CHEN, STUDENT MEMBER, IEEE

Abstract—**A theoretical model considering the effects of Fowler-Nordheim tunneling, image-force lowering, first-order trapping kinetics, impact ionization, and asperity-induced field enhancement has been developed to investigate the ramp-voltage-stressed *I–V* characteristics of the oxide films thermally grown on the polycrystalline silicon. From the ramp-voltage-stressed *I–V* measurements, the important physical parameters such as average field-enhancement factor, effective total trapping density, trap capture cross section, recombination capture cross section, and dielectric breakdown field can be extracted.**

Under a ramp voltage stress, it is shown that the serious asperity effect can lead to a larger leakage current and a weaker dielectric breakdown field, but the serious trapping effect may reduce the leakage current and enlarge the dielectric breakdown field. Moreover, dry O_2 oxidation at a higher temperature and steam oxidation at a lower temperature can result in a better quality poly-oxide because the asperity-induced field enhancement is weakened and the electron trapping effect is slightly increased. Besides, high-temperature dry O_2 oxidation can result in a smaller asperity effect as compared with steam oxidation, and the quality of the poly-oxide is deteriorated when the poly-Si substrate is heavily doped because the asperity effect is enhanced.

I. Introduction

SINCE THE OXIDE films thermally grown on polycrystalline silicon (named poly-oxide) have been widely used in nonvolatile memory devices such as EPROM and EEPROM devices, it is desirable to fabricate high-quality poly-oxide films as these devices are scaled down. The prerequisites for a high-quality oxide film are smaller leakage current and stronger dielectric field strength. However, these characteristics are concerned with electron trapping [1]–[4], positive charge generation, and asperity-induced field enhancement [4]–[11]. Therefore, it is useful to develop a method so that the poly-oxide films can be characterized both qualitatively and quantitatively.

Ramp-voltage-stressed *I–V* measurement has been shown to be a useful technique to investigate the electron trapping [6], [12], [13] and the dielectric field strength [13] of oxide films grown on a single-crystalline silicon substrate. A simple model considering the effects of electron trapping and electric field enhancement of the poly-oxide films has been developed [4], based on a combination of the conventional Fowler–Nordheim conduction mechanism, first-order trapping kinetics, and nonuniform distribution of injection current. However, since the interface between the poly-oxide and its electrode is extremely rough with various bumps, protuberances, and inclusions, it is hard to determine the shape and, further, the dimensions (i.e., height and width) of the asperities.

In this paper, a theoretical model including the effects of modified Fowler–Nordheim tunneling, image-force lowering, first-order trapping kinetics, impact ionization, and asperity-induced field enhancement has been developed to analyze the ramp-voltage-stressed *I–V* characteristics of poly-oxide films. Based on this model, not only electron trapping and the dielectric field strength but also the field-dependent average field-enhancement factor pertaining to the poly-oxide films can be well evaluated. The most prominent feature of the developed model is that the determination of the field-dependent average field-enhancement factor can be simply and accurately calculated from the experimental data without regard to the actual shapes and dimensions of the asperities.

Moreover, poly-oxide films thermally grown in dry O_2 and steam ambients at various temperatures have been fabricated and analyzed theoretically. In addition, the effects of doping types and concentrations in the poly-Si substrate upon the quality of the poly-oxide films have also been investigated and analyzed.

II. Theoretical Model

The carriers flowing through the poly-oxide layer under an external bias are mainly due to electron tunneling from the cathode electrode but not to the holes from the anode electrode because the holes have a larger barrier height and a heavier effective mass. The electrons injected into the conduction band of the oxide layer are governed by the Fowler–Nordheim tunneling mechanism [14]. Compared with oxide films thermally grown on single-crystalline silicon, the most prominent characteristics of oxide films thermally grown on polycrystalline silicon are the asperities and bumps located at the interface between the oxide layer and its electrode [4]–[11]. Therefore, as the

Manuscript received August 26, 1986; revised February 21, 1987. This work was supported under grants from the Electronics Research and Service Organization, the Industrial Technology Research Institute, and the National Science Council, Republic of China.

The authors are with the Institute of Electronics, College of Engineering, National Chiao-Tung University, Hsin-Chu, Taiwan, Republic of China.

IEEE Log Number 8714645.

0018-9383/87/0700-1590$01.00 © 1987 IEEE

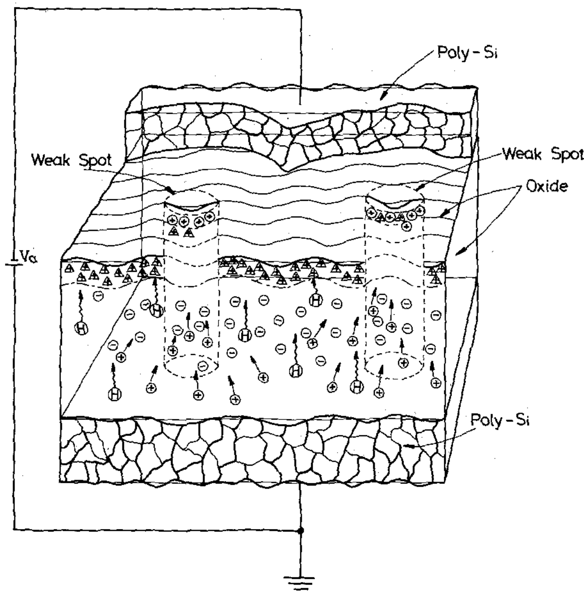

Fig. 1. A theoretical model showing electron trapping, positive charge generation, and asperity-induced weak spots. ⊖ represents the trapped electron; ⊕ represents the positive ions generated from impact ionization; ⊕ represents the neutral species; △ represents the positive charges generated from the diffusion of neutral species and the broken bond at the interface.

electrons tunnel from the poly-Si film into the oxide conduction band under high-field stress, aside from the electron trapping and positive charge generation effects [13], the asperity effect that results in local field enhancement should be considered. Fig. 1 shows schematically the structure of the oxide films thermally grown on the poly-Si in which the area with a locally enhanced electric field is called the weak spot, which is in contrast to the robust area. Besides the asperity effect, the electric field enhancement may be due to nonuniform trap distribution, impurity segregation at the poly-Si grain boundary regions [15], highly mobile positive ions [16], [17], and, especially, locally thin areas.

The energy-band diagrams describing the weak spots and the robust area under different electric fields are shown in Fig. 2(a) through (d). Following previous concepts [13], [18], the electron traps and the trapped electrons are assumed to be distributed uniformly in a plane that is parallel to the cathode-electrode/poly-oxide interface with a distance represented by the trapped electron centroid $\overline{X}_n$. Similarly, the generated positive ions are assumed to be distributed in a plane that is closer to the cathode-electrode/poly-oxide interface with a distance represented by the generated positive ion centroid $\overline{X}_p$. In addition, the positive charges aggregated near the cathode electrode within the robust area and the weak spots are assumed to be resulted from the diffusion of neutral species such as atomic hydrogen [19]–[21] or excitons [22] created by bond-breaking through energetic avalanche-injected electrons and trapped by the dangling bonds at the interface as well as the broken bond at the interface during the passage of heating electrons [23]–[25]. Furthermore, the positive ions generated from band-to-band and/or trap-to-band impact ionization are assumed to be amassed near the cathode electrode within the weak spots due to the locally enhanced electric field.

Considering the effect of electric field enhancement, the Fowler–Nordheim tunneling current density across the potential barriers shown in Fig. 2(a) through (d) has the following form:

$$j(t) = \frac{q^2 m[\mu(E)\, E_c(t)]^2}{16\pi^2 \hbar m^* \Phi_b(\mu, E_c)} \cdot T_p \tag{1}$$

where m^* is the effective mass of the tunneling electrons in oxide and is assumed to be 0.5 m; $\hbar$ is Planck's constant divided by 2π; q is the electronic charge; $E_c(t)$ is the cathode electric field; E is the average electric field across the oxide layer; $\mu(E)$ is the average field-enhancement factor, which is field-dependent; $\Phi_b(\mu, E_c)$ is the barrier height, which considers the image force lowering effect; and T_p is the tunneling probability.

The barrier height including the image-force lowering effect is given by

$$\Phi_b(\mu, E_c) = \Phi_{b0} - \left[\frac{q\mu(E)\, E_c(t)}{4\pi\epsilon_{ox}}\right]^{1/2} \tag{2}$$

where ϵ_{ox} is the dielectric permittivity of the oxide and Φ_{b0} is the intrinsic barrier height.

The tunneling probability calculated by using the WKB approximation has the following relations:

1) For $\Phi_{\overline{X}_p} \geq \Phi_b(\mu, E_c)/\mu(E)$

$$T_{p1} = \exp\left\{-B \cdot \frac{\Phi_b^{3/2}(\mu, E_c)}{E_c(t)}\right\} \tag{3}$$

where $B = -4/3\hbar\mu(E)\,(2m^*q)^{1/2}$ and $\Phi_{\overline{X}_p} = E_c(t)\,\overline{X}_p$.

2) For $\Phi_{\overline{X}_p} < \Phi_b(\mu, E_c)/\mu(E) \leq \Phi_{\overline{X}_n}$

$$T_{p2} = T_{p1} \exp\left\{-B[\Phi_b(\mu, E_c) - \mu(E)\,\Phi_{\overline{X}_p}]^{3/2} \cdot \left(\frac{1}{E_m(t)} - \frac{1}{E_c(t)}\right)\right\} \tag{4}$$

where $E_m(t)$ is the electric field in the middle region and $\Phi_{\overline{X}_n} = E_c(t)\,\overline{X}_p + E_m(t)(\overline{X}_n - \overline{X}_p)$.

3) For $\Phi_{\overline{X}_n} < \Phi_b(\mu, E_c)/\mu(E) \leq \Phi_{T_{ox}}$

$$T_{p3} = T_{p2} \exp\left\{-B[\Phi_b(\mu, E_c) - \mu(E)\,\Phi_{\overline{X}_n}]^{3/2} \cdot \left(\frac{1}{E_a(t)} - \frac{1}{E_m(t)}\right)\right\} \tag{5}$$

where $E_a(t)$ is the anode electric field and $\Phi_{T_{ox}} = E_c(t)\,\overline{X}_p + E_m(t)(\overline{X}_n - \overline{X}_p) + E_a(t)(T_{ox} - \overline{X}_n)$.

4) For $\Phi_{T_{ox}} < \Phi_b(\mu, E_c)/\mu(E)$

$$T_{p4} = T_{p3} \exp\left\{-B\,\frac{[\Phi_b(\mu, E_c) - \mu(E)\Phi_{T_{ox}}]^{3/2}}{E_a(t)}\right\}. \tag{6}$$

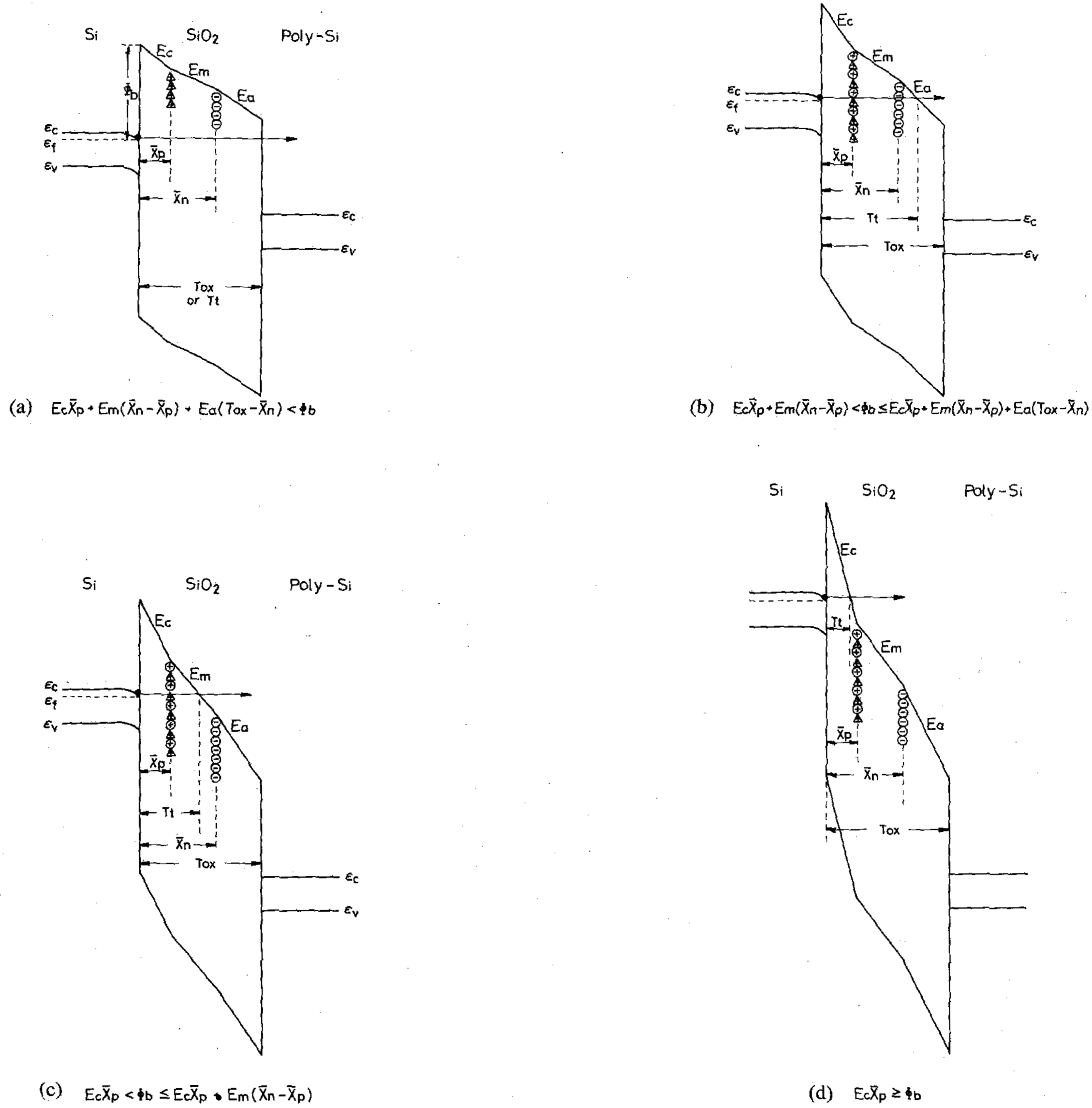

Fig. 2. Energy-band diagrams under different bias voltages.

Note that $E_m(t)$ and $E_a(t)$ are correlated to the cathode electric field $E_c(t)$ via the following equations:

$$E_c(t) = \frac{V_a(t) - \phi_{ms} - \phi_s(t)}{T_{ox}} - \frac{qn_t(t)}{\epsilon_{ox}} \cdot \left(1 - \frac{\overline{X}}{T_{ox}}\right) + \frac{q\theta_i^+(t)}{\epsilon_{ox}}\left(1 - \frac{\overline{X}_p}{T_{ox}}\right) \quad (7)$$

$$E_m(t) = E_c(t) - \frac{q\theta_i^+(t)}{\epsilon_{ox}} \quad (8)$$

$$E_a(t) = E_m(t) + \frac{qn_t(t)}{\epsilon_{ox}} \quad (9)$$

where $V_a(t)$ is the applied voltage, which is equal to γt for the ramp-voltage-stressed I-V measurement and γ is the ramping rate (in volts per second); ϕ_{ms} is the work function difference between two electrodes; $n_t(t)$ is the density of the trapped electrons at $\overline{X}_n$; and $\theta_i^+(t)$ is the density of the effective holes at $\overline{X}_p$.

The electron trapping effect considering the first-order trapping kinetics can be written as

$$\frac{dn_t(t)}{dt} = \frac{\sigma_t j(t)}{q}[N_t - n_t(t)] \quad (10)$$

where N_t and σ_t are the total trapping density and the trap capture cross section of the traps, respectively.

The total positive ions $\theta_{it}^+(t)$ generated from the impact ionization process for the four conditions shown in Fig. 2(a) through (d) can be written as

1) For $\Phi_{\overline{X}_p} \geq \Phi_b(\mu, E_c)/\mu(E)$

$$\theta_{it}^{+}(t) = \frac{\alpha_0}{q}\int_0^t j(t)\Big[(\overline{X}_p - T_t)\exp\left(\frac{-H}{\mu(E)E_c(t)}\right) + (\overline{X}_n - \overline{X}_p)\exp\left(\frac{-H}{\mu(E)E_m(t)}\right) + (T_{ox} - \overline{X}_n)\exp\left(\frac{-H}{\mu(E)E_a(t)}\right)\Big]dt \quad (11)$$

and

$$T_t = \frac{\Phi_b(\mu, E_c)}{\mu(E)E_c(t)}. \quad (12)$$

2) For $\Phi_{\overline{X}_p} < \Phi_b(\mu, E_c)/\mu(E) \le \Phi_{\overline{X}_n}$

$$\theta_{it}^{+}(t) = \frac{\alpha_0}{q}\int_0^t j(t)\left[(\overline{X}_n - T_t)\exp\left(\frac{-H}{\mu(E)E_m(t)}\right) + (T_{ox} - \overline{X}_n)\exp\left(\frac{-H}{\mu(E)E_a(t)}\right)\right]dt \quad (13)$$

and

$$T_t = \overline{X}_p + \frac{\Phi_b(\mu, E_c) - \mu(E)\Phi_{\overline{X}_p}}{\mu(E)E_m(t)}. \quad (14)$$

3) For $\Phi_{\overline{X}_n} < \Phi_b(\mu, E_c)/\mu(E) \le \Phi_{T_{ox}}$

$$\theta_{it}^{+}(t) = \frac{\alpha_0}{q}\int_0^t j(t)(T_{ox} - T_t)\exp\left(\frac{-H}{\mu(E)E_a(t)}\right)dt \quad (15)$$

and

$$T_t = \overline{X}_n + \frac{\Phi_b(\mu, E_c) - \mu(E)\Phi_{\overline{X}_n}}{\mu(E)E_a(t)}. \quad (16)$$

4) For $\Phi_{T_{ox}} < \Phi_b(\mu, E_c)/\mu(E)$

$$\theta_{it}^{+}(t) = 0. \quad (17)$$

Note that α_0 and H are constants pertaining to the impact ionization coefficient α that has the form $\alpha = \alpha_0 \exp(-H/E)$, where E is the electric field and T_t is the tunneling distance.

Considering the electron trapping (or recombination) induced by these positive ions, a rate equation is yielded as follows [13]:

$$\frac{dn_i(t)}{dt} = \frac{\sigma_i j(t)}{q}\left[\theta_{it}^{+}(t) - n_i(t)\right] \quad (18)$$

$$\theta_i^{+}(t) = \theta_{it}^{+}(t) - n_i(t) \quad (19)$$

where σ_i is the recombination capture cross section and $n_i(t)$ is the density of the recombined electrons. Note that the initial conditions for (10) and (18) are $n_t(t = 0)$ and $n_i(t = 0) = 0$, respectively.

The total current across the oxide layer consists of the displacement current, the Fowler–Nordheim tunneling currents through the weak spots and the robust area, and the current due to the movement of the electrons generated from impact ionization, i.e.,

$$I(t) = C_{ox}\frac{dV_a(t)}{dt} + qA_wR_w\left[\frac{d\theta_{it}^{+}(t)}{dt}\right]_w + qA_rR_r\left[\frac{d\theta_{it}^{+}(t)}{dt}\right]_r + A_rR_rj_r(t) + A_wR_wj_w(t) \quad (20)$$

where C_{ox} is the dielectric capacitance of the oxide film; A_w and A_r are the mask areas of the weak spots and the robust area, respectively; R_w and R_r are the ratios of the actual injection area to the mask area of the weak spots and the robust area, respectively; $j_w(t)$ and $j_r(t)$ are the Fowler–Nordheim tunneling current densities through the weak spots and the robust area, respectively; and $[d\theta_{it}^{+}(t)/dt]_w$ and $[d\theta_{it}^{+}(t)/dt]_r$ are the electron generation rates due to impact ionization within the weak spots and the robust area, respectively.

For the oxide films thermally grown on the poly-Si substrate, it can be assumed that the total area is composed of the miscellaneous bumps, protuberances, and inclusions due to the grains formed within the poly-Si substrate so that the robust area is actually absent. Therefore, the total current across the poly-oxide layer becomes

$$I(t) = C_{ox}\frac{dV_a(t)}{dt} + qAR\frac{d\theta_{it}^{+}(t)}{dt} + ARj(t) \quad (21)$$

where A is the total mask area and R is the ratio of the actual injection area to the total mask area.

The I–V characteristics of the poly-oxide layer can be obtained by combining (1) through (21). Since these equations form a nonlinear system, it is necessary to solve them by using the numerical method.

III. Computer Simulations and Discussions

A computer program using the fourth-order Runge–Kutta–Gill numerical method was set up to simulate these nonlinear differential equations. In addition to electron trapping and recombination as well as the dielectric breakdown field concerned with the SiO_2 films grown on the single-crystalline silicon substrate [13], the electric field enhancement of the poly-oxide layer due to the asperity effect deserves noting, especially when the samples are biased by a ramp voltage.

A. Average Field-Enhancement Factor

Fig. 3 shows the simulation results for the I–V characteristics of a poly-oxide layer with a thickness of 700 Å. The basic physical parameters used in Figs. 3 through 7 are listed in Table I, in which the constants α_0 and H are obtained from the impact ionization coefficient of the oxide [26], [27]. As can be seen, the harmful effects of field enhancement are the larger leakage current and the weaker dielectric field strength accompanied by the increase of the field-enhancement factor. Defining the starting electric field E_s to be the electric field that the Fowler–Nordheim tunneling current surmounts the constant displace-

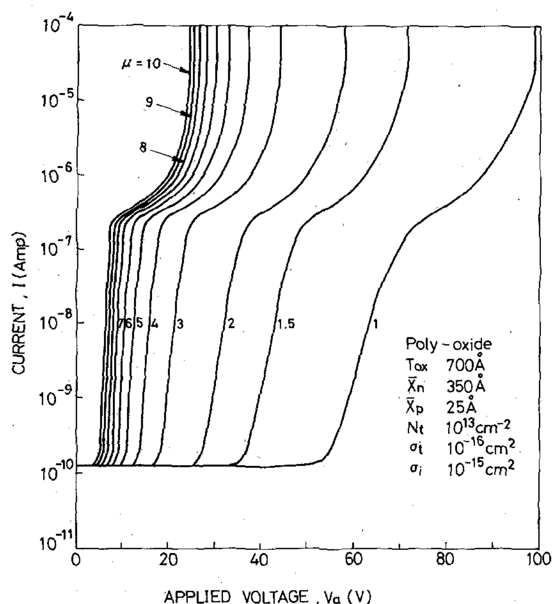

Fig. 3. Computer simulations using the average field-enhancement factor as a parameter for the 700-Å poly-oxide layer.

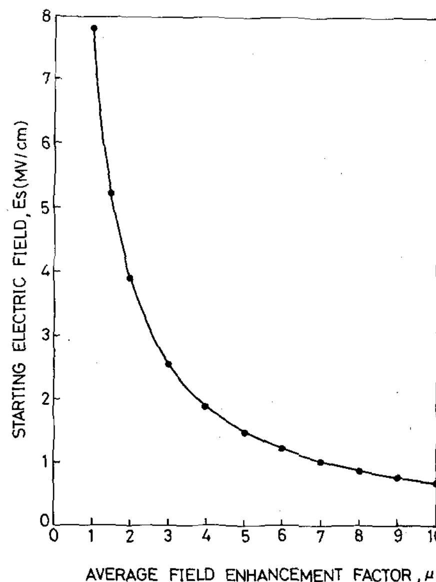

Fig. 4. Starting electric field versus average field-enhancement factor for the 700-Å poly-oxide layer.

TABLE I
PHYSICAL PARAMETERS USED IN FIGS. 3 THROUGH 7

T_{ox} (Å)	$\bar{X}_n$ (Å)	$\bar{X}_p$ (Å)	σ_i (cm²)	N_t (cm⁻²)	σ_t (cm²)	RA (cm²)	γ (v/s)	μ	α_0 (1/cm)	H (MV/cm)
700	350	25	10^{-15}	10^{13}	10^{-16}	1.4×10^{-3}	1	3	3.3×10^{6}	78

ment current, the relationship governing the starting electric field and the average field-enhancement factor can be deduced from Fig. 3 and the result is shown in Fig. 4. The very large slope of the curve shown in this figure as the average field-enhancement factor increases a little above unity indicates that the field enhancement is very sensitive when the electrode deviates slightly from the planar structure; however, the sensitivity attains saturation at the large average field-enhancement factor region (say above 5).

B. Trap Capture Cross Section

Fig. 5 shows the simulation results for the poly-oxide film with an average field-enhancement factor of 3 and a trap capture cross section σ_t ranging from 10^{-18} to 10^{-13} cm^2. Similar to the results concerned with the SiO_2 films grown on the single-crystalline Si substrate [13], the magnitude of the trap capture cross section σ_t pertaining to the poly-oxide films can be determined from the level of the trapping ledge. A larger trap capture cross section leads to a faster electron trapping rate, which in turn lowers the cathode and middle electric fields and thus lessens the leakage current.

C. Effective Total Trapping Density

Fig. 6 shows the simulation results for a poly-oxide film with an average field-enhancement factor of 3 and an effective total trapping density N_t ranging from 1×10^{11} to 5×10^{13} cm^{-2}. It is shown that a larger effective total trapping density N_2 results in a smaller leakage current and a stronger dielectric field strength. This fact is due to decreases of the cathode and middle electric fields with an amount proportional to the density of the trapped electrons as revealed from (7) and (8); consequently, the Fowler–Nordheim tunneling current is lessened. Moreover, since the trapping ledge exhibits a distinct shape as the effective total trapping density N_t changes, as a result, the magnitude of the effective total trapping density N_t can be determined from the trapping ledge of the experimental measurements.

The simulation results for the breakdown field of poly-oxide films with an effective total trapping density N_t and an average field enhancement factor μ as parameters are shown in Fig. 7. As depicted from this figure, the asperity-induced field enhancement weakens the dielectric field strength and the weakening rate is doubled even though the average field-enhancement factor μ is increased from 1 to 2. Additionally, the dielectric field strength is enhanced as the effective total trapping density N_t is increased. This phenomenon is especially prominent when the effective total trapping density is above 1×10^{13} cm^{-2}.

IV. EXPERIMENTAL PROCEDURE AND MEASUREMENTS

Silicon p-type wafers of ⟨100⟩ orientation with a resistivity of about 10 Ω · cm were used as the starting materials. After the standard cleaning process, the SiO_2 layer with a thickness of about 2500 Å was thermally grown on the Si substrate. Undoped poly-Si films of about 5000

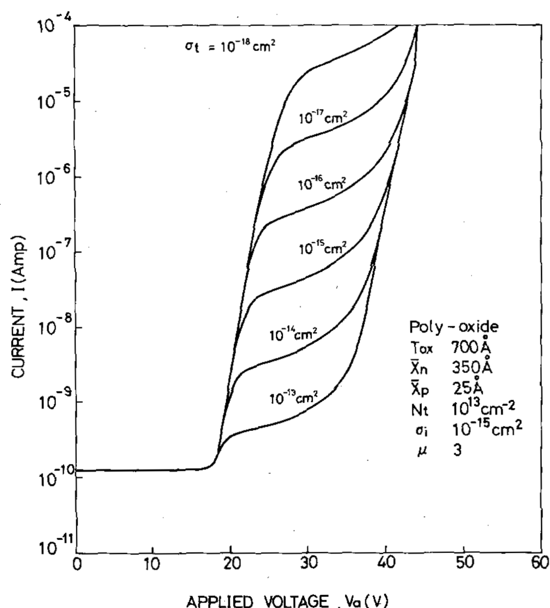

Fig. 5. Computer simulations using the trap capture cross section as a parameter for the 700-Å poly-oxide layer.

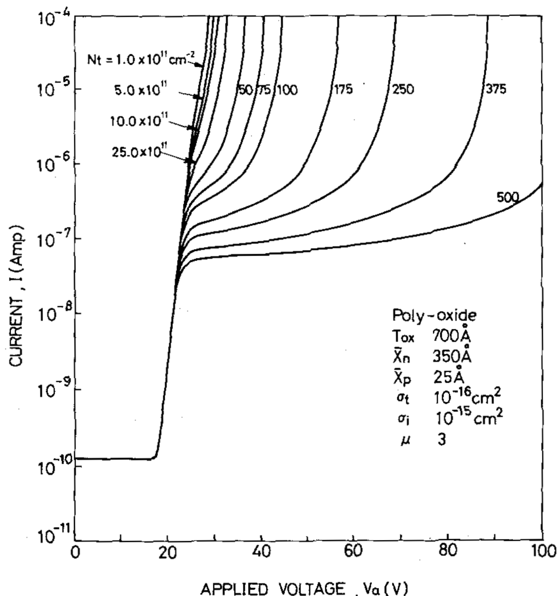

Fig. 6. Computer simulations using the effective total trapping density as a parameter for the 700-Å poly-oxide layer.

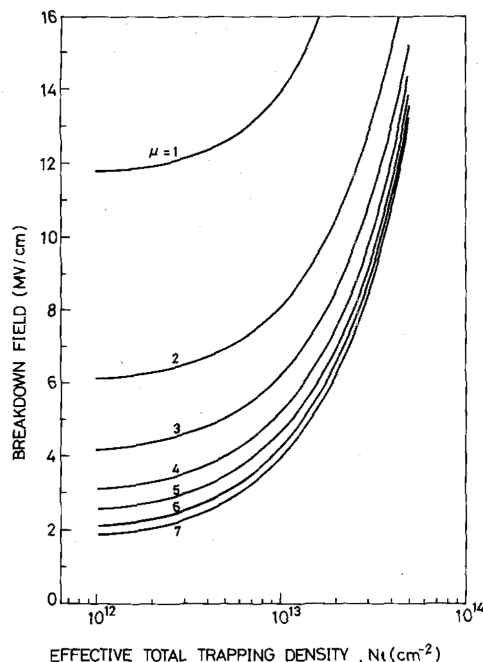

Fig. 7. Breakdown field versus effect total trapping density with the average field-enhancement factor as a parameter.

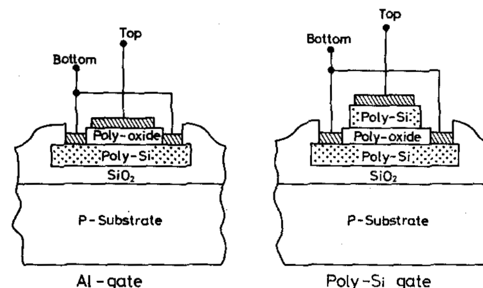

Fig. 8. The structures of the finished samples.

Å were deposited on the oxide layer by thermal decomposition of silane in a low-pressure chemical-vapor deposition (LPCVD) reactor operated at 650°C. Some wafers were doped with phosphorus at 1000°C for 10 min using the $POCl_3$ source; the others were implanted with phosphorus and boron ions with doses from 10^{11} to 10^{15} cm^{-2} at 100 and 90 keV, respectively. Thermal oxidation of the poly-Si films was performed at various temperatures ranging from 900 to 1100°C in dry O_2 and steam ambients. For the samples with the top-electrode made of poly-Si, a second layer of poly-Si was deposited on the wafers and then doped with phosphorus. A pure Al film was evaporated onto the wafers by using a resistive tungsten filament in a vacuum system. The deposited Al film was then photoengraved and etched to form the contact pattern. Finally, the wafers were sintered in forming gas at 450°C for 20 min. The finished structures are shown in Fig. 8.

The average thickness of the poly-oxide layer was measured by an interferometer. The ramp-voltage-stressed *I–V* characteristics was measured by using a Hewlett-Packard 4140B picoammeter controlled by a desk-top computer. A scanning electron microscope (SEM) also was used to observe the surface morphology of the test samples.

V. Experimental Results and Computer Simulations

A. Determination of the Average Field-Enhancement Factor

The ramp-voltage-stressed *I–V* characteristics of SiO_2 grown on a single-crystalline Si substrate with an average field-enhancement factor μ equal to unity have been well simulated [13]. However, for the poly-oxide films, ramp-voltage-stressed *I–V* characteristics cannot be simulated by using a single average field-enhancement factor because the dimensions of the asperities are extremely ran-

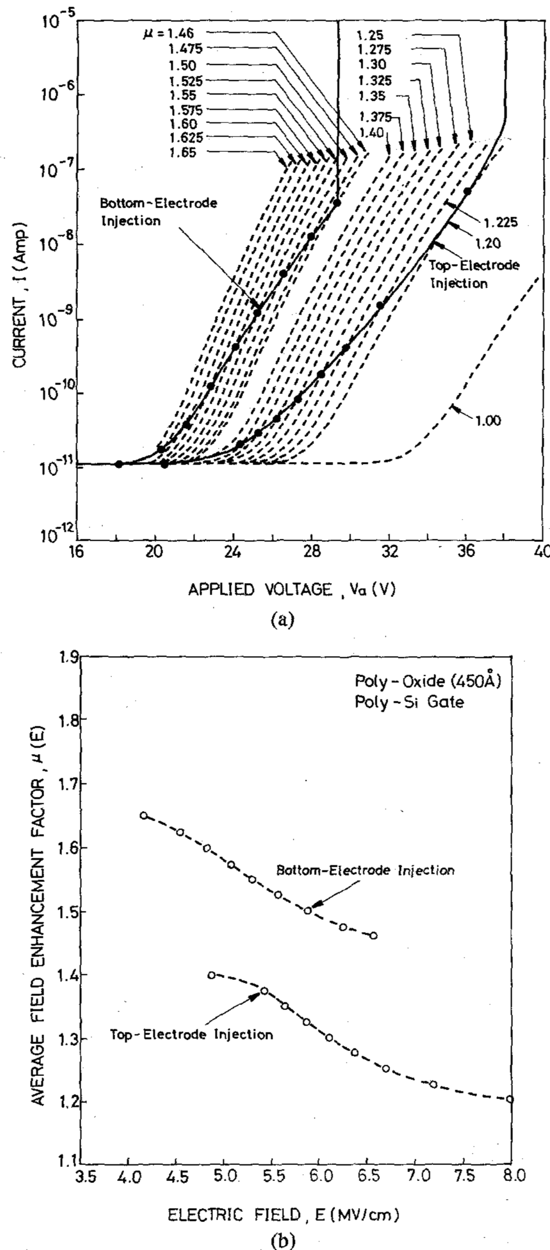

Fig. 9. (a) The ramp-voltage stressed I–V characteristic curves for the 450-Å poly-oxide layer under the bottom- and top-electrode injections and the computer simulations showing the method to determine the average field enhancement factors; (b) the average field enhancement factors extracted from the curve shown in (a).

dom and complicated and the trap distribution is nonuniform: thus, the average field-enhancement factor should be field-dependent. This can be clarified from Fig. 9(a) where the ramp-voltage-stressed I–V characteristics of the 450°-Å poly-oxide layer are simulated by changing the average field-enhancement factor. Note that the bottom- and top-electrode injections represent the injection of electrons into the poly-oxide film from the bottom electrode and the top electrode, respectively. From the intersections of the simulated curves with the experimental curves, the average field-enhancement factor can be determined and the results are shown in Fig. 9(b).

It is clearly seen that the field enhancement is larger for bottom-electrode injection than for top-electrode injection. We attribute this phenomenon to the serious texture roughness, such as the bumps and protuberances of the bottom interface resulted from locally enhanced oxidation at the grain boundaries. On the other hand, the average field-enhancement factor is found to be reduced as the electric field increases. The elements affecting the average field enhancement of poly-oxide films include asperity and electron trapping effects. In order to extract the average field-enhancement factors resulting mainly from the asperities, the Fowler–Nordheim tunneling region of the I–V curve as shown in Fig. 9(a), which always appears before the appearance of the trapping ledge as shown later in Fig. 10, must be used. As the applied voltage across the poly-oxide film increases, the emitting area of the cathode electrode will increase in a nonlinear fashion due to the enlargement of the emitting area pertaining to the asperities with a larger field-enhancement factor coupled with the appearance of the asperities with a smaller field-enhancement factor. This fact would lead to a smaller average field-enhancement factor [4], [28]–[30]. Therefore, the decrease of the average field enhancement factor with the increase of the electric field can be explained.

B. Electron Trapping and Positive Charge Generation

Electron trapping and positive ion generation have been found in SiO_2 film under a high field stress [18]–[25]. In order to observe the electron trapping and the positive ion generation in the poly-oxide layer, a constant current with a density of 2.86×10^{-5} A/cm^2 was used to stress the samples for 90 s which is very near the average time to breakdown of 92 s. Then, thermal detrapping at 350°C for 30 min was performed to remove the trapped electrons from the poly-oxide film so that the positive ions that are left could be measured. Ramp-voltage-stressed I–V measurements were performed by increasing linearly the applied voltage from 0 V to the point where dielectric breakdown takes place. Fig. 10 shows the experimental results for the 390-Å poly-oxide film. It should be noticed that the five curves were obtained by measuring five different samples. After stressing, the measured I–V curve (b) is shifted positively to the fresh one (a). This suggests that the electron trapping occurs during a constant current stress. After stressing and detrapping, the measured I–V curve (c) shifts negatively to the fresh one, which is attributed to the enhanced cathode field by the left positive ions. On the other hand, when a reverse bias is applied to the stressed and thermally detrapped sample, the measured I–V curve (e) is found to be smaller than the fresh one (d). Since the cathode electric field can be enhanced with a magnitude of $(q\theta_i^+(t)/\epsilon_{ox})(1 - \overline{X}_p/T_{ox})$ due to positive ion accumulation, it can be concluded that the positive ions generated under a high-field stress are aggregated near the cathode electrode. The smaller leakage current in the I–V curve (e) when compared with curve (d) is due to the new traps formed by the left positive ions near the anode electrode. This fact lowers the cathode electric field and leads to a smaller tunneling current.

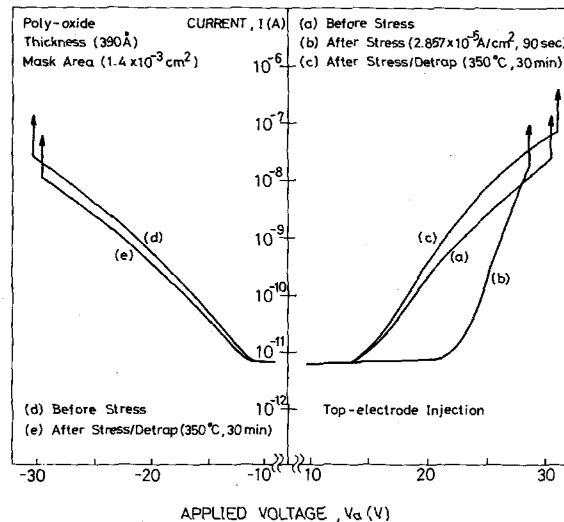

Fig. 10. The ramp-voltage-stressed I–V characteristic curves for the 390-Å poly-oxide layer with and without stressing and detrapping.

Taking the electron trapping and positive charge generation effects of the thin SiO_2 films into account [13], [18], [27], it is interesting to find that the poly-oxide films have the same effects as the thin SiO_2 films grown on single-crystalline substrates.

C. Effects of Oxidation Ambients

Fig. 11(a) and (b) shows the ramp-voltage-stressed I–V characteristic of oxide films thermally grown on polycrystalline Si films at different temperatures in dry O_2 and steam ambients, respectively. Note that the top electrode is made of Al and the samples are biased for bottom-electrode injection. The average field-enhancement factors $\mu(E)$ extracted from these figures are plotted in Fig. 11(c). In addition, the physical parameters used in the theoretical simulations are listed in Table II. The values of the barrier height ϕ_{b0} and the work function difference ϕ_{ms} used in the calculations are chosen to be 3.15 and 0.2 eV [5], respectively. The trapped electron centroid $\overline{X}_n$ is assumed to be one half of the poly-oxide thickness to avoid the highly complicated situations concerned with each sample. The generated positive charge centroid $\overline{X}_p$ is assumed to be 25 Å. Moreover, the procedure for extracting the physical parameters (R, $\mu(E)$, σ_t, N_t, and σ_i) of the poly-oxide film is shown in Fig. 12. Since the actual area for Fowler–Nordheim tunneling from the irregular asperities is correlated to the magnitude of current flow in a complicated manner, our calculations are performed by fixing the area ratio R to a value determined from the displacement current region where the current is approximately proportional to the actual area. The trap capture cross section σ_t and the effective total trapping density N_t are determined from the level and shape of the trapping ledge in the ramped I–V characteristics, respectively, as clearly shown in Figs. 5 and 6. The recombination capture cross section σ_i is determined from the point where the dielectric breakdown takes place [13]. Finally, the product of the trap capture cross section σ_t and the effective total trapping density N_t is used to indicate the degree of the electron trapping effect.

Several important aspects addressed from these figures are:

1) The asperity-induced field enhancement for the poly-oxide films grown in dry O_2 ambient is reduced greatly as the oxidation temperature increases, while a reverse trend is obtained for the poly-oxide films grown in steam ambient. Furthermore, when the oxidation temperature is equal to or larger than 1000°C, the dry O_2 oxidation leads to a smaller field-enhancement factor than the steam oxidation. The surface morphologies of these poly-oxide layers can be observed from the SEM photographs shown in Fig. 13. It can be seen that the dimensions of the asperities are larger for higher oxidation temperatures. According to the grain size growth mechanism [31], the grain size is enlarged as the oxidation temperature increases. However, the asperities with a larger height-to-width ratio are attached to the smaller grain size for dry O_2 oxidation and the larger grain size for steam oxidation. For dry O_2 oxidation, the lower oxidation temperature leads to surface-reaction-controlled oxidation, which gives linear increase in the oxide thickness (T_{ox}) with respect to the oxidation time (t). However, a parabolic increase of the oxide thickness with the diffusion-controlled relationship $T_{ox} \propto t^{0.5}$ is expected for a higher oxidation temperature. Therefore, the oxidant can penetrate more deeply into the grain boundaries at lower oxidation temperature, resulting in a larger height-to-width ratio. For steam oxidation, the grain growth is as severe as compared to that of dry O_2 oxidation and, furthermore, the faster oxidation rate pertaining to higher temperatures causes the oxidant to penetrate deeper into the grain boundaries. This gives a larger height-to-width ratio of the asperities at higher oxidation temperature.

2) The trapping effect becomes more prominant for the poly-oxide films grown in dry O_2 ambient at higher oxidation temperature, whereas a reverse trend is found for

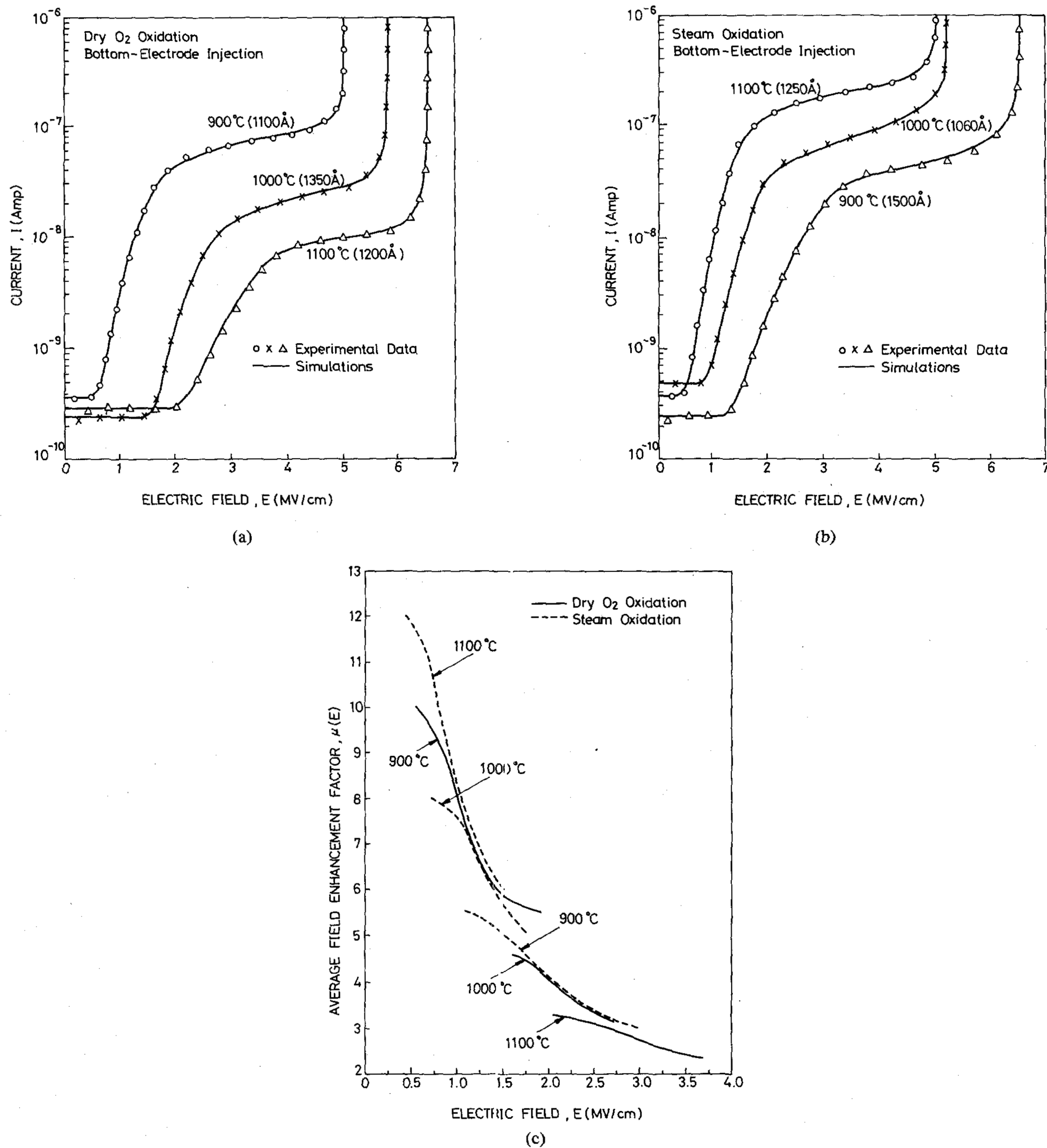

Fig. 11. The ramp-voltage-stressed I–V characteristic curves and theoretical simulations for the poly-oxide films grown in (a) dry O_2 and (b) steam ambients at different temperatures; (c) the average field enhancement factors extracted from the curves shown in (a) and (b).

steam oxidation. Considering the traps originated from the dopants, the oxidation rate of steam oxidation is faster than the phosphorus diffusion rate; and this trend is more obvious at a lower oxidation temperature; therefore, the phosphorus dopants are apt to be trapped in the grown oxide, resulting in a more serious trapping effect. For dry O_2 oxidation, the phosphorus dopants may diffuse into the unoxidized poly-Si film and the diffusion rate is faster at higher temperatures. The increase of the phosphorus concentration in the poly-Si film can enhance the oxidation rate; thus, more phosphorus dopants may be trapped in the grown oxide once the oxidation rate overcomes the phosphorus diffusion rate, which can lead to a more serious trapping effect.

3) The recombination capture cross section is about the same for various oxidation ambients and temperatures.

D. *Effects of Doping Concentration*

The ramp-voltage-stressed I–V characteristics of poly-oxide implanted with different phosphorus and boron doses are shown in Fig. 14(a) and (b), respectively. Fig. 14(c) shows the extracted average field-enhancement fac-

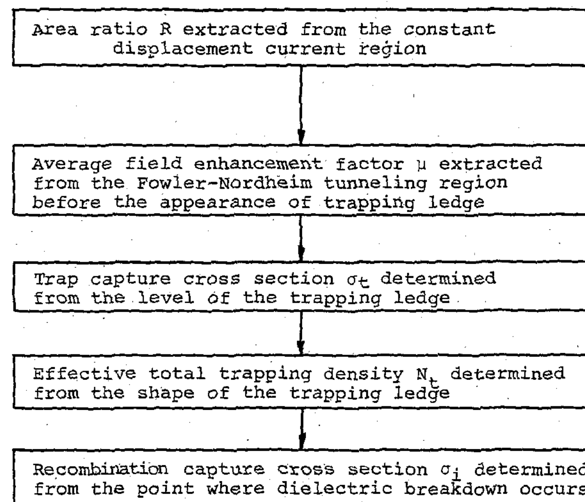

Fig. 12. The flowchart showing the procedure for determining the physical parameters from the experimental data.

TABLE II
PHYSICAL PARAMETERS USED IN FIG. 11(a) AND (b)

Ambient	Temp (°C)	T_{ox} (Å)	$\overline{X}_n$ (Å)	$\overline{X}_p$ (Å)	σ_i (cm²)	σ_t (cm²)	N_t (cm⁻²)	R	$\sigma_t N_t$
	900	1100	500	25	7×10^{-14}	1.0×10^{-15}	8×10^{12}	0.66	8×10^{-3}
Dry O_2	1000	1350	665	25	7×10^{-14}	4.4×10^{-15}	7.5×10^{12}	0.73	3.3×10^{-2}
	1100	1200	600	25	7×10^{-14}	9.7×10^{-15}	6.8×10^{12}	0.89	6.6×10^{-2}
	1100	1250	625	25	7×10^{-14}	3.5×10^{-16}	9.6×10^{12}	0.51	3.36×10^{-3}
Steam	1000	1060	530	25	7×10^{-14}	9.3×10^{-16}	9.1×10^{12}	0.70	8.46×10^{-3}
	900	1500	750	25	7×10^{-14}	1.2×10^{-15}	8.7×10^{12}	0.94	1.04×10^{-2}

tor $\mu(E)$ and Table III lists the physical parameters used in the theoretical calculations. As can be seen from these figures, the phosphorus and boron doses lead to similar trends in the I-V characteristics. The effects can be summarized as: 1) The heavier doping results in a more serious asperity effect, which is ascribed to the faster oxidation rate occurring at the grain boundaries of the heavily doped poly-Si films. 2) The trapping effect is slightly released as the doping increases. 3) The recombination capture cross section shows small differences for various dopants and concentrations.

Note that the electron capture probabilities deduced from grown poly-oxide films vary from 10^{-2} to 10^{-3}, which are much larger than those (10^{-5}–10^{-6}) deduced from thin thermal oxide films grown on silicon substrates [13], [32]. The major reasons are due to the larger thicknesses (1000–2000 Å) of the grown polyoxide films and the properties of polysilicon substrate.

VI. CONCLUSIONS

In this paper, we have proposed a theoretical model to characterize poly-oxide films under different process conditions. Several important effects such as Fowler-Nordheim tunneling, image-force lowering, first order trapping kinetics, impact ionization, and asperity-induced field enhancement are considered in this model. Based on this model, the average field-enhancement factor describing the asperity effect can be well evaluated. Some important conclusions obtained from the theoretical simulations are: 1) The serious asperity effect can enlarge the leakage current and then weaken the dielectric field strength. 2) The larger effective total trapping density can enhance the dielectric field strength and then reduce the leakage current. 3) The larger trap capture cross section can yield a faster trapping rate so that the leakage current is reduced.

The electron trapping and the positive charge aggregation near the cathode electrode under a high-field stress have been observed by using constant current stress, thermal detrapping, and ramp-voltage-stressed I-V measurements. The asperity effect has been found to be more serious for the poly-oxide/bottom-electrode interface when compared with the poly-oxide/top-electrode interface. It is found that the oxide films grown in dry O_2 ambient show a smaller leakage current and a stronger dielectric field strength as the oxidation temperature increases, due to the increase of the trapping effect and the decrease of the asperity effect. However, a reverse trend is obtained

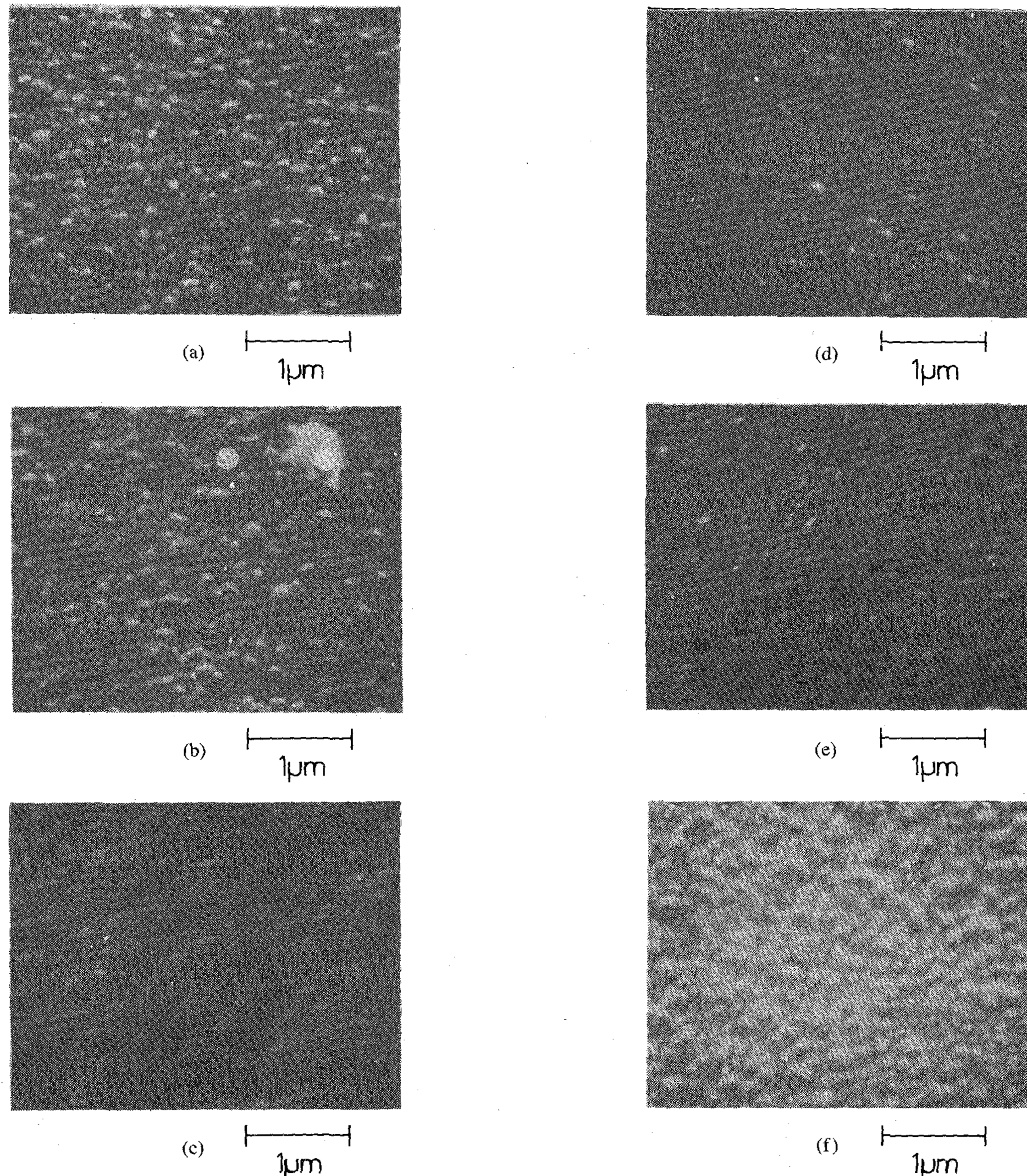

Fig. 13. The SEM photographs showing the surface morphology of the poly-Si films on which the poly-oxide layers have been removed for dry O_2 oxidation at (a) 900°C, (b) 1000°C, and (c) 1100°C; for steam oxidation at (d) 900°C, (e) 1000°C, and (f) 1100°C.

for the poly-oxide grown in steam ambient. For poly-Si films implanted with different phosphorus and boron doses, a common trend shows that heavier doping can lead to a larger leakage current and a weaker dielectric field strength, due to the increase of the asperity effect.

ACKNOWLEDGMENT

Special thanks are given to Dr. C. T. Shih and C. C. Chang for their stimulating discussions.

REFERENCES

[1] D. J. DiMaria, D. R. Young, and D. W. Ormond, "Use of electron-trapping region to reduce leakage currents and improve breakdown characteristics of MOS structures," *Appl. Phys. Lett.*, vol. 31, pp. 680–682, Nov. 1977.
[2] H. S. Lee and C. H. Feng, "High-electric-field-generated electron traps in oxide grown from polycrystalline silicon," *Appl. Phys. Lett.*, vol. 37, pp. 1080–1082, Dec. 1980.
[3] P. A. Heimann, S. P. Murarka, and T. T. Sheng, "Electrical conduction and breakdown in oxides of polycrystalline silicon and their correlation with interface texture," *J. Appl. phys.*, vol. 53, pp. 6240–6245, Sept. 1982.
[4] G. Groeseneken and H. E. Maes, "A quantitative model for the conduction in oxides thermally grown from polycrystalline silicon," *IEEE Trans. Electron Devices*, vol. ED-33, pp. 1028–1042, July 1986.
[5] D. J. DiMaria and D. R. Kerr, "Interface effects and high conductivity in oxides grown from polycrystalline silicon," *Appl. Phys. Lett.*, vol. 27, pp. 505–507, Nov. 1975.
[6] R. M. Anderson and D. R. Kerr, "Evidence for surface asperity mechanism of conductivity in oxide grown on polycrystalline silicon," *J. Appl. Phys.*, vol. 48, pp. 4834–4836, Nov. 1977.
[7] E. A. Irene, E. Tierney, and D. W. Dong, "Silicon oxidation studies: Morphological aspects of the oxidation of polycrystalline silicon," *J.*

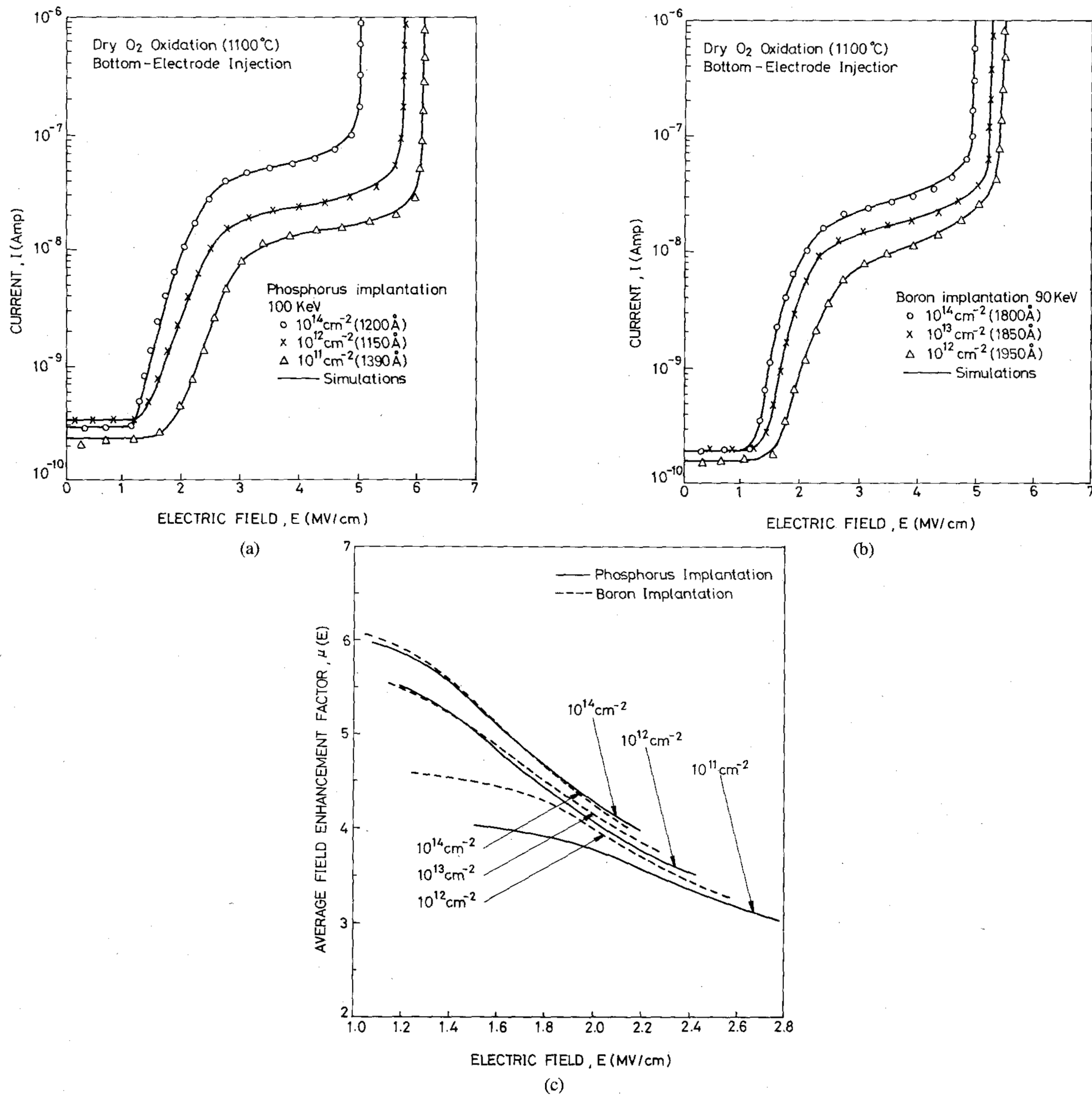

Fig. 14. The ramp-voltage-stressed I–V characteristic curves and theoretical simulations for the poly-oxide films implanted with different amounts of (a) phosphorus and (b) boron doses and oxidized in dry O_2 ambient; (c) the average field-enhancement factors extracted from the curves shown in (a) and (b).

TABLE III
PHYSICAL PARAMETERS USED IN FIG. 14(a) AND (b)

Dopant	Dose (cm^{-2})	T_{ox} (Å)	$\overline{X}_n$ (Å)	$\overline{X}_p$ (Å)	σ_i (cm^2)	σ_t (cm^2)	N_t (cm^{-2})	R	$\sigma_t N_t$
	10^{14}	1200	600	25	7×10^{-14}	1.2×10^{-15}	8.3×10^{12}	0.78	9.96×10^{-3}
P	10^{12}	1150	575	25	7×10^{-14}	1.9×10^{-15}	10^{13}	0.82	1.9×10^{-2}
	10^{11}	1390	695	25	7×10^{-14}	2.8×10^{-15}	9.2×10^{12}	0.85	2.58×10^{-2}
	10^{14}	1800	900	25	7×10^{-14}	1.5×10^{-15}	8.1×10^{12}	0.72	1.22×10^{-2}
B	10^{13}	1850	925	25	7×10^{-14}	2.2×10^{-15}	7.8×10^{12}	0.82	1.72×10^{-2}
	10^{12}	1950	975	25	7×10^{-14}	4.1×10^{-15}	7.1×10^{12}	0.87	2.91×10^{-2}

Electrochem. Soc., vol. 127, pp. 705–713, Mar. 1980.

[8] H. R. Huff, R. D. Halvorson, T. L. Chiu, and D. Guterman, "Experimental observations on conduction through polysilicon oxide," *J. Electrochem. Soc.*, vol. 127, pp. 2482–2488, Nov. 1980.

[9] H. S. Lee and S. P. Marin, "Electrode shape effects on oxide conduction in films thermally grown from polycrystalline silicon," *J. Appl. Phys.*, vol. 51, pp. 3746–3750, July 1980.

[10] H. Sunami, M. Koyanagi, and N. Hashimoto, "Intermediate oxide formation in double-polysilicon gate MOS structure," *J. Electrochem. Soc.*, vol. 127, pp. 2499–2506, Nov. 1980.

[11] R. B. Marcus, T. T. Sheng, and P. Liu, "Polysilicon / SiO_2 interface microtexture and dielectric breakdown," *J. Electrochem. Soc.*, vol. 129, pp. 1282–1289, June 1982.

[12] D. J. DiMaria, R. Ghez, and D. W. Dong, "Charge trapping studies in SiO_2 using high current injection from Si-rich SiO_2 films," *J. Appl. Phys.*, vol. 51, pp. 4830–4841, Sept. 1980.

[13] C. F. Chen and C. Y. Wu, "A characterization model for ramp-voltage-stressed *I–V* characteristics of thin thermal oxides grown on silicon substrate," *Solid-State Electron.*, vol. 29, pp. 1059–1068, Oct. 1986.

[14] M. Lenzlinger and E. H. Snow, "Fowler–Nordheim tunneling into thermally grown SiO_2," *J. Appl. Phys.*, vol. 40, pp. 278–287, Jan. 1969.

[15] P. S. D. Lin, R. B. Marcus, and T. T. Sheng, "Leakage and breakdown in thin oxide capacitors-correlation with decorated stacking faults," *J. Electrochem. Soc.*, vol. 130, pp. 1878–1883, Sept. 1983.

[16] T. H. Distefano, "Dielectric breakdown induced by sodium in MOS structures," *J. Appl. Phys.*, vol. 44, pp. 527–528, Jan. 1973.

[17] D. J. DiMaria, F. J. Feigl, and S. R. Butler, "Trap ionization by electron impact in amorphous SiO_2 films," *Appl. Phys. Lett.*, vol. 24, pp. 459–461, May 1974.

[18] I. C. Chen, S. E. Holland, and C. Hu, "Electrical breakdown in thin gate and tunneling oxides," *IEEE Trans. Electron Devices*, vol. ED-32, pp. 413–422, Feb. 1985.

[19] F. J. Feigl, D. R. Young, D. J. DiMaria, S. Lai, and J. Calise, "The effects of water on oxide and interface trapping charge generation in thermal SiO_2 films," *J. Appl. Phys.*, vol. 52, pp. 5665–5682, Sept. 1981.

[20] R. Gale, "Hydrogen migration under avalanche injection of electrons in Si metal-oxide-semiconductor capacitors," *J. Appl. Phys.*, vol. 54, pp. 6938–6942, Dec. 1983.

[21] C. T. Sah, J. Y. C. Yun, and J. J. T. Tzou, "Study of the atomic models of three donor-like traps on oxidized silicon with aluminum gate from their processing dependences," *J. Appl. Phys.*, vol. 54, pp. 5864–5879, Oct. 1983.

[22] A. Hartstein and D. R. Young, "Identification of electron traps in thermal silicon dioxide films," *Appl. Phys. Lett.*, vol. 38, pp. 631–633, Apr. 1981.

[23] H. L. Hughes, "Radiation-induced perturbations of the electrical properties of the silicon-silicon dioxide interface," *IEEE Trans. Nucl. Sci.*, vol. NS-16, pp. 195–202, Dec. 1969.

[24] C. W. Gwyn, "Model for radiation-induced charge trapping and annealing in the oxide layer of MOS devices," *J. Appl. Phys.*, vol. 40, pp. 4886–4892, Nov. 1969.

[25] T. P. Ma, "Oxide thickness dependence of electron-induced surface states in MOS structures," *Appl. Phys. Lett.*, vol. 27, pp. 615–617, Dec. 1975.

[26] M. Knoll, D. Bräunig, and W. R. Fahrner, "Comparative studies of tunnel injection and irradiation on metal oxide semiconductor structures," *J. Appl. Phys.*, vol. 53, pp. 6946–6952, Oct. 1982.

[27] I. C. Chen and C. Hu, "Hole trapping and breakdown in thin SiO_2," *IEEE Electron Device Lett.*, vol. EDL-7, pp. 164–167, Mar. 1986.

[28] T. J. Lewis, "High field electron emission from irregular cathode surfaces," *J. Appl. Phys.*, vol. 26, pp. 1405–1410, Dec. 1955.

[29] R. K. Ellis, H. A. R. Wegener, and J. M. Caywood, "Electron tunneling in non-planar floating gate memory structure," in *IEDM Tech. Dig.*, pp. 749–752, Dec. 1982.

[30] R. K. Ellis, "Fowler–Nordheim emission from non-planar surfaces," *IEEE Electron Device Lett.*, vol. EDL-3, pp. 330–332, Nov. 1982.

[31] Y. Wada and S. Nishimatsu, "Grain growth mechanism of heavily phosphorus-implanted polycrystalline silicon," *J. Electrochem. Soc.*, vol. 125, pp. 1499–1504, Sept. 1978,

[32] C. F. Chen and C. Y. Wu, "A characterization model for constant-current-stressed voltage-time characteristics of thin thermal oxides grown on silicon substrate," *J. Appl. Phys.*, vol. 60, pp. 3962–3944, Dec. 1986.

*

Ching-Yuan Wu (S'69–M'72) was born in Taiwan, Republic of China, on March 18, 1946. He received the B.S. degree from the Department of Electrical Engineering, National Taiwan University, Taiwan, Republic of China, in 1968 and the M.S. and Ph.D. degrees from the State University of New York (SUNY) at Stony Brook, in 1970 and 1972, respectively.

During the 1968–1969 academic year, he served in the Chinese Air Forces as a Second Lieutenant. During the 1972–1973 academic year, he was appointed as a Lecturer at the Department of Electrical Sciences, SUNY, Stony Brook. During the 1973–1975 academic years, he was a Visiting Associate Professor at National Chiao-Tung University (NCTU), Taiwan, Republic of China. In 1976, he became a Full Professor in the Department of Electronics and the Institute of Electronics, NCTU. During 1974–1980, he was the Director of Engineering Laboratories and Semiconductor Research Center, NCTU. He was a principal investigator of the National Electronics Mass Plan—Semiconductor Devices and Integrated-Circuit Technologies, during 1976–1979. He was the Director of the Institute of Electronics, NCTU, during 1978–1984. Since 1984, he has been the Dean, College of Engineering, NCTU. He has also been the Research Consultant of the Electronics Research and Service Organization (ERSO), ITRI, and the Academic Advisory Member of the Ministry of Education, Republic of China. He has been the Coordinator of Microelectronics Research and Development Committee, National Science Council (NSC), Republic of China. His research activities have been in semiconductor device physics and modeling, and integrated-circuit designs and technologies. His present research interest focus on small-geometry devices in VLSI, CMOS latchup, and new devices and technologies. He has published over 120 papers in the semiconductor field.

Dr. Wu is a member of Phi Tau Phi and an Editor of *Journal of the Chinese Institute of Engineers in Electrical Engineering*. He received the Academic Research Award in Engineering from the Ministry of Education (MOE), in 1979; the outstanding Scholar award from the Chinese Educational and Curtural Foundation, Republic of China, in 1985; and the Outstanding Research Professor Fellowship from the MOE and the National Science Council (NSC), Republic of China, during 1982–1986.

*

Chiou-Feng Chen (S'85) was born in Taichung, Taiwan, Republic of China, on September 19, 1956. He received the B.S. degree in electrical engineering from National Cheng-Kung University, Tainan, Taiwan, Republic of China in 1979 and the M.S. degree in electronics engineering from National Chiao-Tung University, Hsin-Chu, Taiwan, Republic of China, in 1981. He is currently working toward the Ph.D. degree at the Institute of Electronics, National Chiao-Tung University. His research interests have been in modeling and characterization of thin oxide, poly-oxide, and EEPROM devices.

From 1981 to 1983, he served as a technical officer in the Chinese Army.